Mean-field calculations of exotic nuclei ground states

G. Co', V. De Donno
Dipartimento di Fisica, Università del Salento, Lecce, Italy and INFN, Sezione di Lecce, Via Arnesano, I-73100 Lecce, Italy

P. Finelli
Dipartimento di Fisica Università di Bologna, Bologna, Italy and INFN, Sezione di Bologna, I-40126 Bologna, Italy

M. Grasso
Insitut de Physique Nucléaire, IN2P3-CNRS, Université Paris-Sud, F-91406 Orsay Cedex, France

M. Anguiano, A. M. Lallena
Departamento de Física Atómica, Molecular y Nuclear, Universidad de Granada, E-18071 Granada, Spain

C. Giusti, A. Meucci, F. D. Pacati
Dipartimento di Fisica Nucleare e Teorica, Università di Pavia, Pavia, Italy and INFN, Sezione di Pavia, Via Bassi 6, I-27100 Pavia, Italy

(Dated: February 8, 2012)

We study the predictions of three mean-field theoretical approaches in the description of the ground state properties of some spherical nuclei far from the stability line. We compare binding energies, single particle spectra, density distributions, charge and neutron radii obtained with non-relativistic Hartree-Fock calculations carried out with both zero and finite-range interactions, and with a relativistic Hartree approach which uses a finite-range interaction. The agreement between the results obtained with the three different approaches indicates that these results are more related to the basic hypotheses of the mean-field approach rather than to its implementation in actual calculations.

PACS numbers: 21.60.Jz, 24.10.Jv, 21.10.Dr, 21.10.Ft, 21.10.Pc

I. INTRODUCTION

The study of the properties of nuclei far from the stability valley is one of the major topics of interest of modern nuclear physics. Wide experimental programs of investigation are planned at nuclear facilities now under construction [1–5] and we expect that, in the next few years, a large amount of data regarding these nuclei will be available. From the theoretical point of view, the main question is whether the theories and the models which have been developed, and tested, to describe stable nuclei will be able to perform well also in the description of these exotic nuclei.

We classify the nuclear theories as ab-initio and effective ones. In the first case, nucleon-nucleon interactions built to describe observed quantities of two-body, and eventually also of three-body, nuclear systems are employed. These theories solve the many-body Schrödinger equation exactly or by making a few and well controlled approximations. In these last years, thanks to the advances of the computing facilities, these theories have been applied to the description of finite nuclear systems [6–13]. Their success in the description of light nuclei reinforces the validity of the basic hypotheses of the non-relativistic description of the nuclear systems. Despite the great progress in the field, the use of these theories for the description of medium and heavy nuclei is still limited because of the complexity of the calculations.

Effective theories are less ambitious. Their approach to the many-body problem is based on the mean-field (MF) assumptions. Effects beyond MF are taken into account in an effective manner by the nucleon-nucleon interaction, whose parameters are chosen to reproduce the values of some basic observable of a wide set of nuclei. Effective theories are used to describe, and predict, nuclear properties different from those chosen to determine the force, as well as the properties of nuclei not included in the fit procedure. The calculations of observables within effective theories

are much simpler, and numerically less involved, than those of the microscopic theories. For these reasons effective theories are widely used in the description of medium and heavy nuclei.

Effective nuclear theories can be classified in two groups: phenomenological and microscopic ones. We call phenomenological those theories, and models, where the MF is globally parametrized with a simple potential ansatz, for example a harmonic oscillator or a Woods-Saxon well. The parameters of these wells are determined to reproduce the experimental values of some ground state properties and, therefore, they change for each nucleus considered. These approaches are extremely useful and powerful if one considers each nucleus individually, as, for example, in the case of the Landau-Migdal theory of finite Fermi systems [14–16]. Unfortunately, the requirement of the experimental knowledge of some ground-state properties of the nuclei under investigation, strongly hinders the use of these phenomenological theories to explore experimentally unknown regions of the nuclear chart.

For this purpose, the microscopic MF theories [17–19] are more promising. In these theories, the only input is the effective nucleon-nucleon interaction, and the MF potential is constructed by using minimization procedures which lead to the Hartree, or to the Hartree-Fock equations when the Pauli principle is explicitly considered. In these approaches the parameters of the effective interaction are chosen by making a global fit of some properties of a large set of nuclei. Since the effective interaction is unique for all the nuclei, microscopic MF approaches are suitable to make predictions for nuclei not yet experimentally identified.

Non relativistic Hartree-Fock (HF) calculations have a long history and tradition in nuclear physics. One of the approaches of major success uses the zero-range Skyrme interaction [20, 21]. Since the original formulation of Skyrme, and the seminal paper of Vautherin and Brink [22], many different parametrizations of the interaction have been proposed. Always in HF framework, a finite-range interaction has been proposed by Gogny and collaborators at the beginning of the 80's [23]. In this case HF calculations are more involved and, consequently, also the fit procedure. For these reasons the number of parametrizations of this interaction available in the literature is much smaller than that of the Skyrme interaction.

The most recent microscopic MF approach appearing in the literature describes the nucleonic motions by using the Dirac, rather than the Schrödinger, equation [24]. In this relativistic approach the nucleon-nucleon interaction is written in terms of an effective Lagrangian which describes the exchange of some mesons whose values of masses and coupling constants are determined to fit some global properties of stable nuclei. Usually, in this approach only the direct interaction matrix elements are considered, and this leads to a set of Dirac-Hartree equations.

A short description of the three different approaches, the details of the interactions used in the calculations, the presentation of the observables we have investigated and of the nuclei we have considered are given in Sec. II. Our results are presented and discussed in Sec. III. Here we first discuss in Sec. III A the results of the infinite asymmetric nuclear matter system. After that, we show how the three approaches behave when they are applied to describe nuclei out of the stability valley, in an experimentally unexplored region of the nuclear chart. We wanted to identify those features of the results depending on the MF basic assumptions and disentangle them from those related to the specific implementation of the MF model. Specifically, we have investigated the properties of a set of 16 nuclei, selected for their specific characteristics. These nuclei can be grouped in four isotopic chains, oxygen, calcium, nickel and tin; therefore our study covers a relatively wide range of masses in the nuclear isotope chart. Since in our calculations we assume spherical symmetry, we have selected the spherical nuclei of each isotope chain, these are the nuclei where the single particle (s.p.) levels are fully occupied. In Sec. III B, we show the results concerning binding and s.p energies of the nuclei we have considered. The most severe test on the predictions of the three different MF models is done in Sec. III C, where we discuss quantities directly connected to the wave functions, i.e. density distributions and response functions. Finally, in Sec. III D, we present some results regarding nuclear radii and neutron skins. After having summarized the main results, we present in Sec. IV our conclusions.

II. THE MODELS

The details of the MF approaches we have adopted in our investigations are presented in various publications, for example in Refs. [22, 23, 25, 26], therefore we do not repeat here the derivation of the various expressions used in our HF and Dirac-Hartree calculations. In this section we give information about the inputs of our calculations, essentially about the effective interactions we have used.

We start with the older, and more exploited, approach: the HF calculations done with the Skyrme interaction. This interaction contains a central, a spin-orbit and a density-dependent term and some velocity-dependent non local components. All of them have zero range, though the last ones can be viewed as an approximation of finite-range. Several parametrization have been introduced in the past decades, many of them presented and discussed in the review of Ref. [27].

In our work we have employed the SLy5 parametrization which has been introduced by the Saclay-Lyon collaboration in the '90s [28–30]. As for the SLy4 interaction, the SLy5 parametrization has been chosen to reproduce binding

energies and root mean squared (rms) radii of several nuclei, and, in addition, some symmetric nuclear matter and neutron matter properties. With respect to the SLy4 force, in the fitting procedure of the SLy5 parameters the terms of the Hamiltonian density depending on the square of the spin-orbit density have not been neglected. The strength of these new terms is determined by those of the velocity-dependent terms. Henceforth, we shall indicate as SLy5 the results obtained with this HF approach.

Also the second MF approach we have adopted is based on non-relativistic HF calculations, but now finite-range interactions are used. The motivations for using interactions with finite range in HF calculations are well discussed in the original paper of Dechargè and Gogny [23], where a new type of effective interaction has been proposed. This interaction, called Gogny force, has finite range in the traditional four central channels and two zero-range terms which are the spin-orbit and the density dependent term.

The original parametrization of the interaction given in Ref. [23], and called D1, was improved with a new one, called D1S [31], which was built to reproduce a larger set of data. This parametrization is the most widely used, but it has the annoying feature to produce a neutron matter equation of state whose energy per nucleon becomes negative at large values of the neutron density. This indicates a problem in the isospin dependent terms of the force. To fix this problem a large fitting project has been developed to reproduce more than two thousand nuclear masses, hundreds of rms charge radii, and also energy gaps [32, 33]. This procedure has produced a new set of parameter values, the D1M force [34] which we have used in our calculations. In the following, we shall indicate as D1M the results obtained with the finite-range HF approach.

The third approach we have used is based on the relativistic mean-field theory, the traditional relativistic field theory where nucleons are treated as Dirac particles moving in several classical meson fields. These fields describe in an average way the interaction produced by the exchange of the corresponding mesons. The theory considers a defined number of mesons whose corresponding parameters, the meson masses and the meson-nucleon coupling constants, are chosen to reproduce empirical data. Conventional relativistic mean-field calculations usually include non-linear self-interaction meson couplings, for the scalar and vector mesons, but, more recently, a new class of relativistic functionals containing density dependent meson-nucleon vertex functions has been introduced. In principle, the functional form of the meson-nucleon vertexes can be deduced from Dirac-Brueckner calculations with realistic free-space nucleon-nucleon interactions [26] but, to have a better agreement with experimental data, in this work we used a phenomenological parametrization of the meson-nucleon coupling called DDME2 [35]. This parametrization has a density dependence for the σ, ω, and ρ meson-nucleon couplings adjusted to reproduce properties of symmetric nuclear matter, neutron matter, and a limited set of spherical nuclei. More details on the Dirac-Hartree approach can be found in Ref. [35]. In the following, we shall indicate as DDME2 the results obtained with this approach.

	Fermi level	
Nucleus	p	n
^{16}O	$1p_{1/2}$	$1p_{1/2}$
^{22}O	$1p_{1/2}$	$1d_{5/2}$
^{24}O	$1p_{1/2}$	$2s_{1/2}$
^{28}O	$1p_{1/2}$	$1d_{3/2}$
^{40}Ca	$1d_{3/2}$	$1d_{3/2}$
^{48}Ca	$1d_{3/2}$	$1f_{7/2}$
^{52}Ca	$1d_{3/2}$	$2p_{3/2}$
^{60}Ca	$1d_{3/2}$	$2p_{1/2}$
^{48}Ni	$1f_{7/2}$	$1d_{3/2}$
^{56}Ni	$1f_{7/2}$	$1f_{7/2}$
^{68}Ni	$1f_{7/2}$	$2p_{1/2}$
^{78}Ni	$1f_{7/2}$	$1g_{9/2}$
^{100}Sn	$1g_{9/2}$	$1g_{9/2}$
^{114}Sn	$1g_{9/2}$	$1g_{7/2}$
^{116}Sn	$1g_{9/2}$	$3s_{1/2}$
^{132}Sn	$1g_{9/2}$	$1h_{11/2}$

Table I: Nuclei investigated in this work and last occupied proton and neutron s.p. levels, the Fermi levels, for each of them.

We conclude this section by presenting the set of isotopes we have chosen to investigate. We list these nuclei in Table I and, for each of them, we indicate the last occupied level, the Fermi level. As already mentioned in

the introduction, we have chosen four isotopic chains, and within each chain we have selected those nuclei where the number of nucleons completely fills the s.p. levels. The deformed Hartree-Fock-Bogoliubov calculations of Refs. [36, 37] confirm the spherical shape of these nuclei, therefore our approaches based on spherical symmetry are adequate to describe them. In these nuclei also the pairing effects are minimized. None of the nuclei considered shows pairing effects in the proton sector. The situation for neutrons is more complicated, since in some of the isotopes considered the pairing is different from zero. We have investigated the relevance of these pairing effects by carrying on Bardeen-Cooper-Schriefer, Hartree-Fock Bogoliubov and relativistic Hartree-Bogoliubov calculations with the three interactions presented above. We found that the effects of the neutron pairing on binding energies, charge and matter rms radii are at most of a few parts in a thousand. These results induced us to neglect the pairing in our study.

All the nuclei we have investigated resulted to be bound, except ^{48}Ni in DDME2 calculations, where the energy of the proton $1f_{7/2}$ level is positive. From the experimental point of view, it seems rather well established that the neutron drip line for the oxygen isotopes starts with ^{26}O [38] and, therefore, ^{28}O should not be bound.

III. RESULTS

A. Infinite matter

The first step of our investigation consists in comparing the predictions of the three MF models for the equation of state (EOS) of infinite nuclear matter. In this study we are interested in comparing the different results at the saturation densities, and how they evolve with increasing densities.

The systems we are studying have translational invariance and constant nucleonic density defined as the sum $\rho = \rho_{\rm p} + \rho_{\rm n}$ of the proton, $\rho_{\rm p}$, and neutron, $\rho_{\rm n}$ densities, both of them also constant. The energy per nucleon $e = E/A$ for asymmetric matter is usually written as a function of even powers of the asymmetry parameter $\delta = (\rho_{\rm n} - \rho_{\rm p})/\rho$,

$$e(\rho,\delta) \,=\, e(\rho,0) \,+\, e_{\rm sym}(\rho)\,\delta^2 \,+\, \mathcal{O}(\delta^4)\,. \tag{1}$$

Around the stability minimum of symmetric nuclear matter, at density ρ_0, the two coefficients of this equation are expanded in powers of the parameter $\epsilon = (\rho - \rho_0)/(3\,\rho_0)$. For symmetric nuclear matter we have

$$e(\rho,0) \,=\, a_V \,+\, \frac{1}{2} K_V\,\epsilon^2 \,+\, \ldots\,, \tag{2}$$

where the term of first order in ϵ, related to the first derivative, is zero because $e(\rho,0)$ has a minimum in ρ_0. In the quadratic term, related to the second derivative, the coefficient defined as

$$K_V \,=\, 9\rho_0^2\,\left.\frac{\partial^2 e(\rho,0)}{\partial\rho^2}\right|_{\rho=\rho_0} \tag{3}$$

is called volume compression modulus. The second coefficient in Eq. (1), i.e. the symmetry energy, is expanded as

$$e_{\rm sym}(\rho) \,=\, a_{\rm sym} \,+\, \mathcal{L}\,\epsilon \,+\, \ldots\,. \tag{4}$$

The coefficient

$$\mathcal{L} \,=\, 3\rho_0\,\left.\frac{\partial e_{sym}(\rho)}{\partial\rho}\right|_{\rho=\rho_0} \tag{5}$$

has recently attracted great attention since it is closely related to some neutron stars properties and to the size of the nuclear neutron skin [39].

We show in Table II the values of some nuclear matter quantities calculated at the saturation density ρ_0, and we compare them with the empirical values and with those obtained in auxiliary field diffusion Montecarlo (AFDMC) [40] and correlated basis function (CBF) [41] calculations by using microscopic nucleon-nucleon interactions of Argonne-Urbana type.

We observe that all the values of the saturation densities and of the energies per nucleon agree within 2% and 0.4%, respectively. The values of K_V are very similar in the two HF calculations (D1M and SLy5), being also close to the commonly accepted empirical value. The value obtained with DDME2 is slightly larger, but in agreement with the result of the microscopic calculations. Also the MF $e_{\rm sym}(\rho_0)$ are rather similar, within 6%, while we observe large differences in the $\mathcal{L}$ values.

	exp	AFDMC	CBF	D1M	SLy5	DDME2
ρ_0	0.16 ± 0.01	0.16	0.16	0.16	0.16	0.15
$e(\rho_0, 0)$	-16.0 ± 0.1	-16.00	-16.00	-16.01	-15.98	-16.13
K_V	220 ± 30	276	269	217	228	278
$e_{\rm sym}(\rho_0)$	30-35	31.3	33.94	29.45	32.66	33.20
$\mathcal{L}$	88 ± 25	60.10	58.08	25.41	48.38	54.74

Table II: Infinite nuclear matter properties for various calculations. The saturation density ρ_0 is expressed in fm^{-3}. All the other quantities in MeV. The auxiliary field diffusion Monte Carlo (AFDMC) results are from Ref. [40], and those of the correlated basis function (CBF) theory from Ref. [41].

In Fig. 1 we show the EOS of pure neutron matter (upper panel), the symmetric nuclear matter (medium panel) and the symmetry energy $e_{\rm sym}$ (lower panel). The three MF calculations produce very different results at large densities. The EOS generated by the SLy5 calculations has a behavior very similar to that of the microscopic ones. The DDME2 calculations produce stiffer EOS in both symmetric nuclear matter and pure neutron matter. The situation for the D1M results is more complicated. In symmetric nuclear matter there is a good agreement with the microscopic EOS, while in pure neutron matter the D1M EOS is the lowest one. The almost flat behavior of the D1M symmetry energy at saturation density produces the low value of $\mathcal{L}$ given in Table II.

In the following section, we investigate if the differences we have pointed out in the nuclear matter results have consequences on finite nuclei observables.

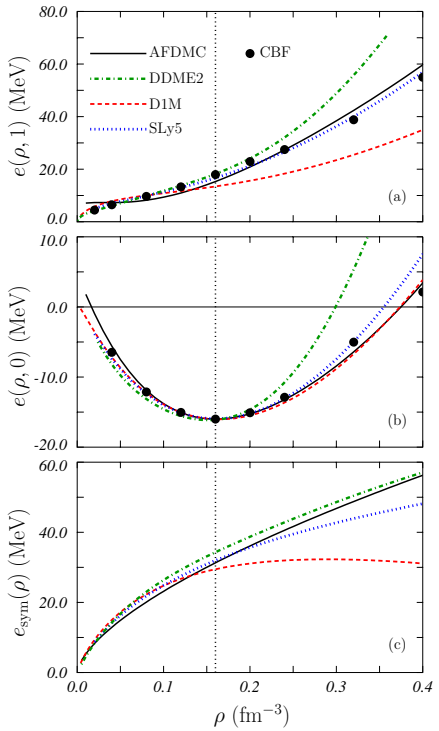

Figure 1: (Color on line) Equation of state for pure neutron matter (a) and symmetric nuclear matter (b), and symmetry energy (c) calculated with different theories. The solid circles represent the correlated basis function results of Ref. [41]. The full black lines show the auxiliary field diffusion Monte Carlo results of Ref. [40]. The other lines show the results of the D1M (dashed red lines), SLy5 (dotted blue lines) and DDME2 (dashed-dotted green lines) calculations. The dotted vertical lines indicate the value of the empirical saturation density $\rho_0 = 0.16$ fm^{-3}.

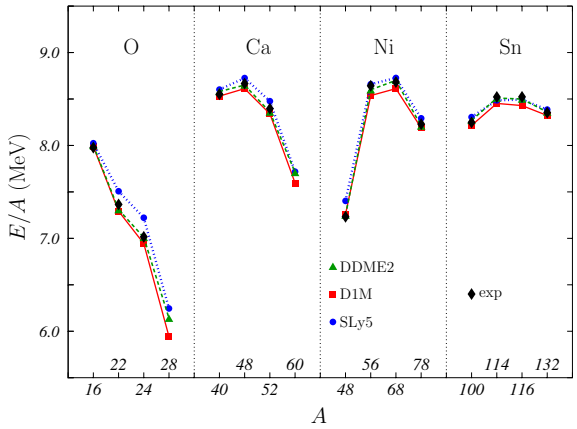

Figure 2: (Color on line) Binding energies per nucleon calculated with the three different MF models and compared with the experimental values [42]. The lines are drawn to guide the eyes.

B. Binding and single particle energies

In the application of the three MF models to the description of finite nuclear systems we first investigate binding and s.p. energies. Binding energies are some of the observables used to chose the values of the interaction parameters in the three models. For this reason, we do not expect large differences between the results obtained for this observable, even though the binding energies of neutron rich nuclei are genuine predictions. The situation is different for the s.p. energies which are not used to determine the force parameters.

In Fig. 2 we compare the binding energies per nucleon given by the various models with the experimental data of Ref. [42]. As expected, the three calculations describe reasonably well these data. We observe that the SLy5 results are systematically higher than those obtained with the other interactions. The D1M results are the most bound, and the DDME2 results are between the two. In any case, the largest relative difference with respect to the experimental data is 0.6%. It is worth pointing out that the three models produce similar binding energies for ^{28}O and ^{60}Ca, that are bound in all our calculations and for which this quantity has not been measured.

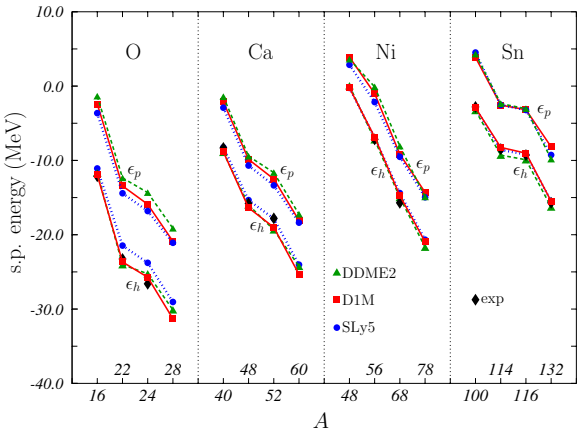

Figure 3: (Color on line) Energies of the s.p. proton levels just below and above the Fermi surface, ϵ_h and ϵ_p respectively. The experimental separation energies [42] are also shown.

In Fig. 3 we show the values of the s.p. energies of the proton levels around the Fermi surface. Specifically, the energies, ϵ_h, of the last occupied hole level of each nucleus indicated in Table I are plotted. In our model, these energies correspond to the proton separation energies $S_{\rm p}$ [43], and, in the figure, we compare them with the experimental values [42]. The results of all the calculations show the same trend, in each isotope chain, the protons become more bound as the neutron number increases. The scale of the figure does not show well the fact, previously remarked, that the energy of the proton $1f_{7/2}$ level in ^{48}Ni is slightly positive in the DDME2 calculation. The detailed comparison

between the various calculations indicates that the SLy5 results are less bound than the other ones. This effect is more evident in the oxygen isotopes, and disappears in heavier nuclei.

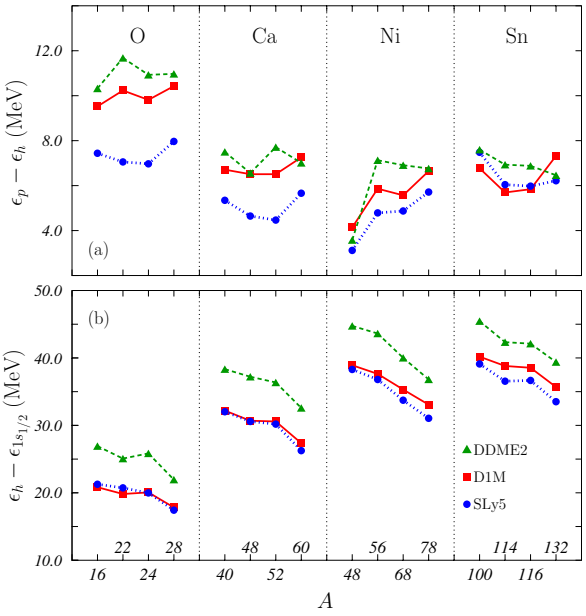

Figure 4: (Color on line) In panel (a) we show the proton energy gap, $\epsilon_p - \epsilon_h$. In panel (b) the energy differences, $\epsilon_h - \epsilon_{1s_{1/2}}$, between the s.p. energy of the least bound proton level and that of the $1s_{1/2}$ level, calculated with the three different MF models.

In Fig. 3 we also show the s.p. energies, ϵ_p, of the proton particle levels, just above the Fermi surface. They are $1d_{5/2}$, $1f_{7/2}$, $2p_{3/2}$ and $1g_{7/2}$ for oxygen, calcium, nickel and tin isotopes respectively. Also in this case we observe a similar trend in the results of all the calculations. In each isotope chain, the values of ϵ_p decrease with increasing neutron number. The results obtained with the SLy5 interaction are more bound than those obtained with the other calculations. Also in this case, the effect is more evident in the oxygen isotopes than in heavier nuclei.

The results shown in Fig. 4 emphasize the differences between the three MF calculations. In panel (a), we show the energy gap $\epsilon_p - \epsilon_h$. In general, SLy5 produces the smallest gaps and DDME2 the largest ones, with few exceptions. The differences between the three calculations become smaller as nuclei become heavier and all of them show a minimum for ^{48}Ni.

In panel (b) of Fig. 4 we show the differences between the s.p. energy of the least, ϵ_h, and most, $\epsilon_{1s_{1/2}}$, bound proton hole levels. As expected, this quantity increases with the number of protons since more s.p. levels must to be arranged in the bound system. It is interesting the fact that, within the same isotope chain, the increase of the neutron number reduces the value of this energy difference and, consequently, increases the density of proton states. The general behavior of the three calculations is the same, but the DDME2 results are consistently larger than those obtained in the non-relativistic calculations.

C. Proton, neutron and matter distributions and electron scattering.

We have seen in the previous sections that the three models produce remarkably different results only in infinite systems at densities much larger than those of the saturation point. The results of the binding and s.p. energies for the isotopes we have investigated are very similar. We want now to investigate the differences between the wave functions generated by the three models. We have conducted this study by calculating matter distributions, radii, and electron scattering cross sections. These observables are more sensitive to the details of the wave functions than the energies.

The results we have obtained for proton, neutron, and matter distributions show the same general features in all isotope chains. As an example of these results, we present here the distributions of the calcium isotopes, where the effects we want to discuss are more extreme with respect to those found in the other nuclei.

We show in Fig. 5 the proton distributions, $\rho_{\rm p}$, of the four calcium isotopes we have considered. There is an excellent agreement between the results of the three calculations at the nuclear surface.

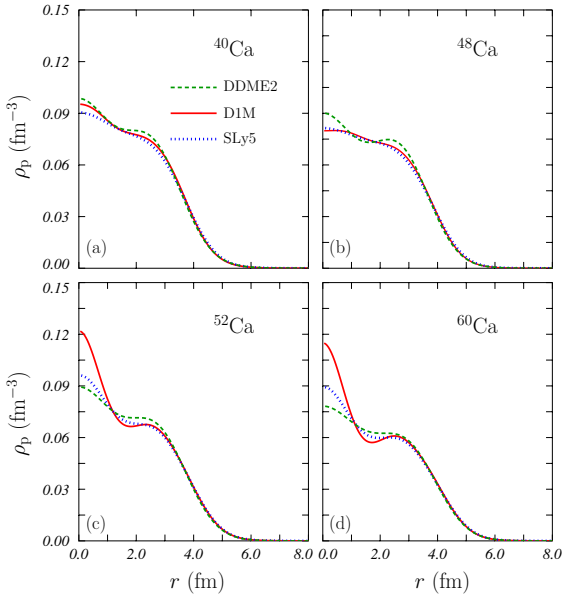

Figure 5: (Color on line) Proton distributions for the various calcium isotopes we have considered. Full, dotted and dashed lines indicate, respectively the D1M, Sly5 and DDME2 results.

In the center of the nucleus, the three calculations produce similar results for ^{40}Ca and ^{48}Ca, but the D1M densities are larger than the other ones in ^{52}Ca and ^{60}Ca nuclei. This behavior is a peculiarity of the D1M parametrization of the Gogny interaction. The results obtained with the D1S force, for example, do not show this feature [44]. The differences with respect to the D1M results shown in Ref. [44] are due to an improvement of the numerical accuracy of the HF calculations.

To investigate this behavior we have analyzed the s wave functions, which, in MF models are the only s.p. wave functions contributing to density at the nuclear center. In calcium isotopes, the differences in the density distributions

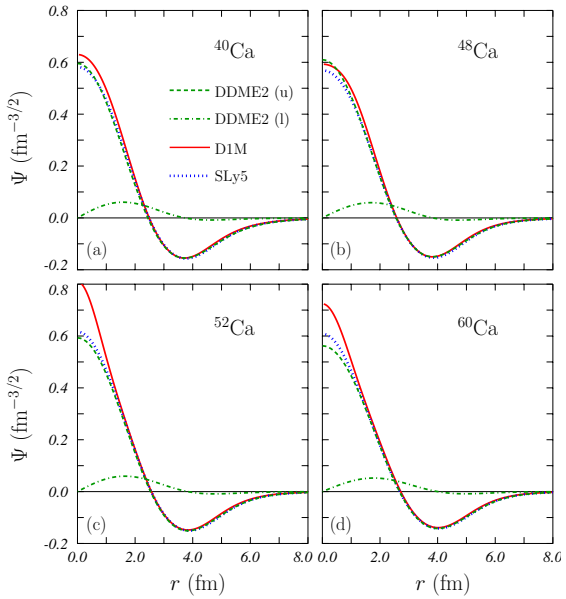

Figure 6: (Color on line) Wave functions of the proton $2s_{1/2}$ levels for the calcium isotopes. Full and dotted lines represent the D1M and SLy5 results, respectively. For the relativistic DDME2 calculation we show both the upper (u) and lower (l) components with dashed and dashed dotted lines.

are mainly due to the $2s_{1/2}$ s.p. wave functions which we show in Fig. 6. Remarkable differences are obtained between D1M waves and those obtained with the other MF approaches for ^{52}Ca and ^{60}Ca, at $r \sim 0$ fm. On the other hand, it is interesting to observe the similarity of these wave functions in the surface region. For the DDME2 calculations, we present in the figure also the lower components of the wave functions.

A possibility of studying details of the s.p. wave functions is offered by (e, e′p) experiments. A long series of high-precision measurements on a wide range of nuclei [45–52] singled out exclusive (e, e′p) knockout reactions, where the emitted proton is measured in coincidence with the scattered electron, as the primary tool to explore the s.p. aspects of the nuclear structure. The theoretical description of the (e, e′p) reaction has been developed within the framework of the non-relativistic distorted-wave impulse approximation (DWIA) [47, 50, 52–54] and relativistic distorted-wave impulse approximation (RDWIA) [55–64], including the distortion produced by the final-state interaction between the outgoing proton and the residual nucleus, which is described in the calculations with non-relativistic or relativistic phenomenological optical potentials, as well as the distortion of the electron wave functions due to the presence of the nuclear Coulomb field. Both DWIA and RDWIA approaches were able to describe to a high degree of accuracy (e, e′p) data on several nuclei in a wide range of different kinematics.

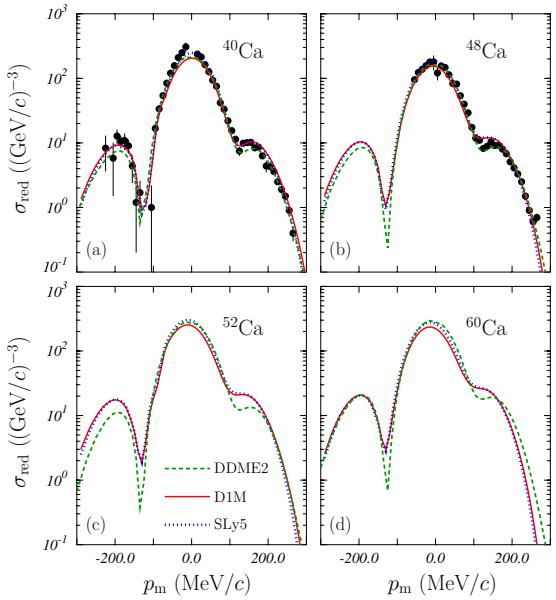

Figure 7: (Color on line) Reduced cross sections for the (e, e′p) process for various calcium isotopes, in parallel kinematics. The proton is emitted from the $2s_{1/2}$ state. The value of the energy of the incident electron is 483.2 MeV, the electron scattering angle 61.52^o, the momentum transfer 450 MeV/c and the energy of the emitted proton 100 MeV. The experimental data (solid circles) of the ^{40}Ca and ^{48}Ca isotopes have been taken from Ref. [65]. The meaning of the lines is the same as in Fig. 5.

We have calculated (e, e′p) cross sections, for the emission of a proton from the $2s_{1/2}$ s.p. level of the calcium isotopes we have considered, under the so-called parallel kinematics of the NIKHEF experiments [65]. In the parallel kinematics the momentum of the emitted proton is kept fixed and taken parallel, or antiparallel, to the direction of the momentum transfer $\mathbf{q}$. Different values of the missing momentum $p_{\rm m}$, which is the recoil momentum of the residual nucleus, are obtained by varying the electron scattering angle and, as a consequence, q. Calculations have been carried out in DWIA and RDWIA, using the s.p. bound-state wave functions obtained in the three MF approaches considered. Details of the calculations are described in Ref. [66]. We notice that RDWIA calculations require four-vector relativistic wave functions for both the initial bound and the final scattering state,as well as a relativistic nuclear current operator. The results of the DWIA and RDWIA calculations are compared in Fig. 7, where the reduced cross sections for the calcium isotopes are drawn as a function of the missing momentum. The reduced cross section is the cross section divided by a suitable kinematic factor [52] and by the elementary electron-proton cross section [67]. In order to reproduce the magnitude of the experimental data, a reduction factor is usually applied to the calculated cross sections. For the results shown in Fig. 7 the reduction factors are 0.57 for ^{40}Ca and 0.58 for ^{48}Ca. No reduction factors have been applied for the other isotopes, where experimental data are not available.

The differences between the various wave functions do not produce relevant changes of the (e, e′p) cross sections in the kinematics considered in Fig. 7. We also remark the excellent agreement between the results of all our calculations and the shape of the experimental reduced cross sections on ^{40}Ca and ^{48}Ca target nuclei. Similar results are also

obtained in [66], where DWIA and RDWIA calculations are performed with different s.p. bound-state wave functions.

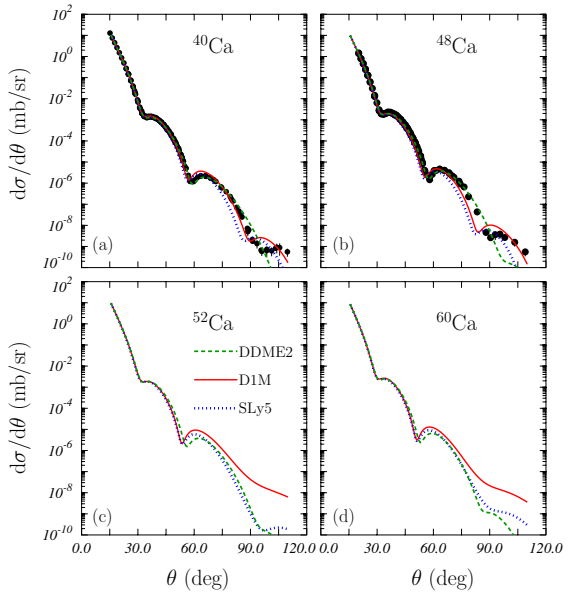

Figure 8: (Color on line) Elastic electron scattering cross sections calculated by using the charge distributions obtained with the three MF approaches we have considered. The experimental data (solid circles) are from Refs. [70–72], for ^{40}Ca, and Ref. [73], for ^{48}Ca. All the data have been rescaled to match an unique electron energy of 400 MeV. The meaning of the lines is the same as in Fig. 5.

Experimental information about proton distributions is obtained by the elastic electron scattering off nuclei. In this case, the tool is more sensitive to the global charge distribution of the nucleus than to that of specific s.p. wave functions. We have calculated elastic electron scattering cross sections in the distorted-wave Born approximation [68, 69] by using the proton density distributions of Fig. 5. The charge densities have been obtained by folding the proton densities with an electromagnetic nucleon form factor of dipole form. We have verified that there are not significant differences if other, and more sophisticated, nucleon form factors are used.

In Fig. 8 we show the elastic electron scattering cross sections, calculated for an electron energy of 400 MeV, as a function of the scattering angle. We compare our calculations with the experimental data of Refs. [70–72] for the ^{40}Ca nucleus and of Refs. [73, 74] for the ^{48}Ca nucleus. It is interesting to notice that, for the calcium isotopes considered, the cross sections calculated with the different models start to differ at about 60^o, which, in the actual kinematics, corresponds to a momentum transfer value of 400 MeV/c.

These results indicate that transferred momenta larger than 400 MeV/c are necessary to produce phenomena able to disentangle the differences between the s.p. wave functions. The (e, e′p) cross sections in the NIKHEF kinematics [65] just reach this value and are not sensitive to the differences in the $2s_{1/2}$ wave functions.

We have addressed great attention to the proton distributions because of their connection with observables quantities, and also because they contain information on the effective proton-neutron interaction. Without this part of the interaction all the proton densities of an isotope chain should be the same. We discuss now the neutron distributions of the nuclei we have chosen to study.

In Fig. 9 we show these distributions, $\rho_{\rm n}$, for the calcium isotopes we have studied. Obviously, the densities become more extended with increasing neutron number. Also in this case, we observe that, for each nucleus, the densities obtained with the different calculations have very similar surface behaviors. As in the proton case, the differences between the various results are remarkable in the center of the nuclei. The major fluctuations of the densities are shown by the D1M results and mainly in the two isotopes, ^{52}Ca and ^{60}Ca, where also the proton distributions have shown large differences with respect to the results of the other calculations. While in the proton case the distributions presented a peak in the nuclear center, in the neutron case we observe a hole.

We show in Fig. 10 the matter distributions, $\rho_{\rm m}$, for the four calcium isotopes obtained as a sum of proton and neutron distributions. In this case, the agreement between the results of all the calculations is much better than that obtained by considering separately proton and neutron distributions. This similarity is due to the fact that all the interactions used in the three calculations depend on the total matter density, and not separately on the proton or neutron densities.

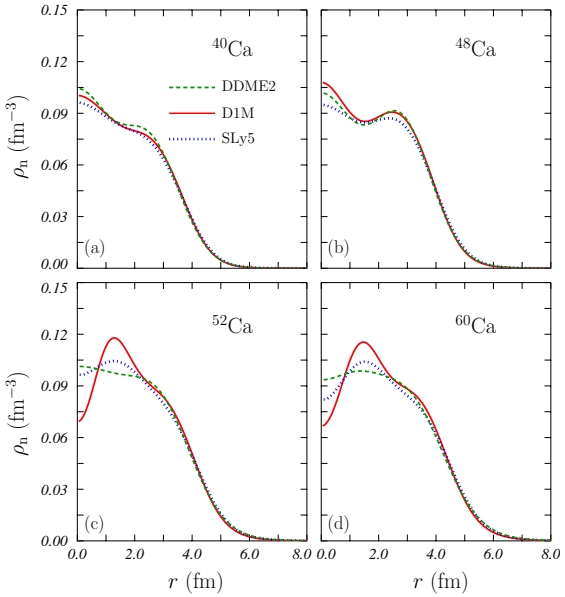

Figure 9: (Color on line) Neutron distributions for the various calcium isotopes we have considered. The meaning of the lines is the same as in Fig. 5.

The general features of the proton and neutron distributions we have presented for the calcium isotopes are similar to those obtained in the other isotope chains. There is excellent agreement at the surface while differences are obtained in the nuclear interior. These differences are larger for the separated proton and neutron densities than in the case of the total matter density.

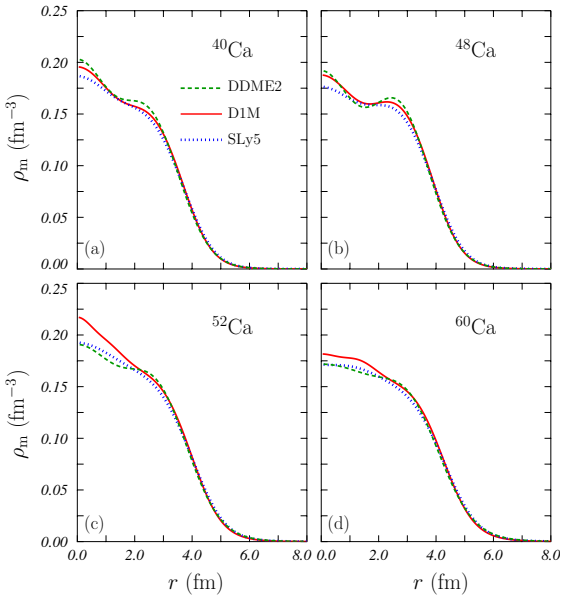

Figure 10: (Color on line) Matter distributions for the various calcium isotopes we have considered. The meaning of the lines is the same as in Fig. 5.

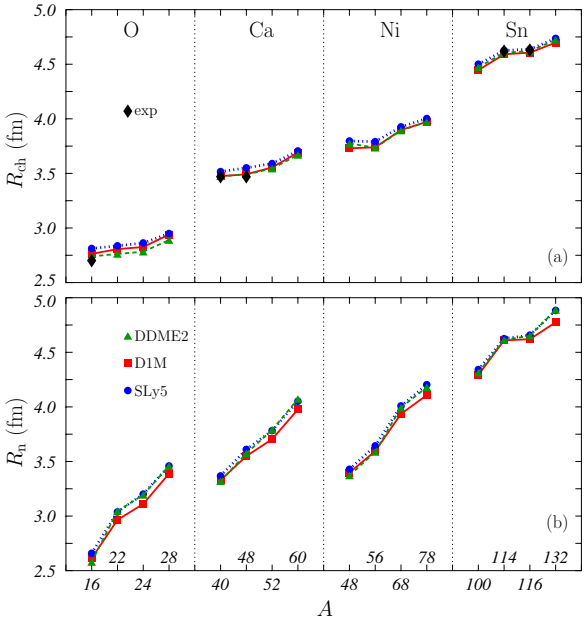

Figure 11: (Color on line) In the panels (a-d) we show the rms charge radii compared with the empirical values of Ref. [75]. In panels (e-f) we show the rms neutron radii.

D. Nuclear radii and neutron skin

The matter distribution results discussed in the previous sections show differences between the various calculations in the nuclear interior, while there is an excellent agreement at the surface. As a consequence, the values of the rms radii calculated with the three approaches are very similar as we show in Fig. 11. In panel (a) the rms charge radii are compared with the available experimental values [75]. In panel (b) the rms neutron radii are shown.

The agreement between the results of the various calculations is remarkable. The maximum relative differences appear between DDME2 and SLy5 calculations in ^{24}O for R_{ch} (2.8%) and ^{16}O for R_n (3.0%). The maximum absolute difference is 0.1 fm (in ^{132}Sn for R_n). We observe a general trend of the SLy5 calculations to produce radii slightly larger than those obtained by the other calculations, these are, however, small differences as we have already pointed out.

The behavior of the neutron rms radii is rather obvious. The increasing number of neutrons increases the radius values. It is interesting to notice that these values are almost the same for ^{40}Ca and ^{48}Ni which have same number of neutrons. The D1M rms neutron radii are slightly smaller than the other ones. This tendency is more evident for the Sn isotopes.

The charge radii agree very well with the available experimental values [75]. We have compared our results with the values obtained by using the semi-empirical expression given by Eq. (4) of Ref. [76], and also found excellent agreement. In this case, the largest difference is of about 1.9% with the SLy5 results in the ^{16}O nucleus.

The behavior of the charge radii is not as obvious as that of the neutron radii, since here the number of particles, protons, remains the same in each isotope chain. In all the isotope chains we have investigated, we observe a small increase with increasing neutron number. This effect is due to the proton-neutron interaction which rearranges the proton distributions to optimize the global matter distribution with respect to the energy minimum.

In Fig. 12 we show the neutron skins, defined as difference between neutron and proton rms radii $R_n - R_p$ [76, 77], as a function of the relative neutron excess, $(N - Z)/A$. The various symbols identify the different isotope chains.

We found negative values for the neutron skins of the four self-conjugate nuclei, i.e. those with $N = Z$, and for the ^{48}Ni nucleus, where the number of neutrons is smaller than that of the protons. The effect in the self-conjugate nuclei is a clear evidence of the Coulomb repulsion, as it shown by the increase of the phenomenon with increasing proton number. We go from -0.02 fm in ^{16}O to -0.08 fm in ^{100}Sn. For these self-conjugate nuclei, the three MF calculations produce neutron skin values which differ for less than 0.01 fm.

In each isotope chain, the value of the neutron skins increases with increasing neutron number, as expected. The results of the three MF calculations slightly differ with increasing neutron number. The three types of calculations show an almost linear correlation between neutron skins and the relative neutron excess. The full lines show the linear

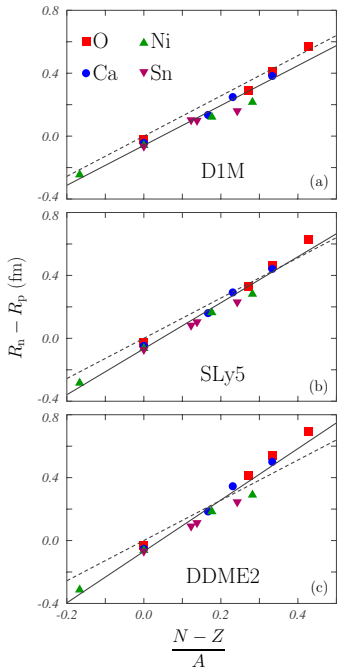

Figure 12: (Color on line) Neutron skins calculated with the three different approaches as a function of the relative neutron excess. The full lines show a linear fit do the data and the dashed lines the predictions of the model proposed in Ref. [77].

fits to the results of our calculations. The three models produce different values on the slopes of the line, specifically 1.31 fm for D1M, 1.46 fm for SLy5 and 1.63 fm for DDME2. Since for $N = Z$ the three models give essentially the same values, this indicates that, for nuclei with neutron excess, the neutron skins obtained with the DDME2 interaction are larger than those obtained with Sly5, and these last ones are larger than those obtained with D1M. The nuclear matter properties given in table II show a direct link between these results and $e_{\rm sym}$ and $\mathcal{L}$, as pointed out in the literature (see e.g. Refs. [17, 39, 78, 79]).

In the figure, the dashed lines show the predictions of the model proposed in Ref. [77] where the neutron skins are described as

$$R_{\rm n} - R_{\rm p} \, = \, 1.28 \, \frac{N-Z}{A} \, . \tag{6}$$

The model has a reasonable agreement with our linear fits, especially with that of the D1M results.

Another interesting fact emerging from the results of Fig. 12, is that, for similar values of the relative neutron excess, lighter nuclei have larger neutron skins than heavier nuclei. This is evident in the case of self-conjugate nuclei, where the sequence O, Ca, Ni, Sn is exactly reproduced by all the calculations. The behavior of the neutron skins is an interesting topic which deserves further investigation.

IV. CONCLUSIONS

In this work, we have compared the results of three different implementations of the nuclear MF model in a region of the nuclear chart which has not been yet experimentally explored. We have investigated whether the three different MF approaches provide different results, as it happens in infinite nuclear matter at high density values. We have studied the ground state properties of 16 spherical nuclei. Specifically, we have calculated binding and s.p. energies, and also quantities more sensitive to the details of the wave functions, such as density distributions and elastic and inelastic electron scattering cross sections. The general good agreement between the results of the three models indicates that these results are more related to the basic hypotheses of the MF model rather than to the details of their implementation, such as the type of interaction or the relativistic, or non-relativistic, approach.

More specifically, some of the relevant results common to all the calculations we have presented are listed here below.

1. The properties of infinite nuclear matter at the saturation density in the three approaches are very similar and reproduce rather well the empirical values. The only exception is $\mathcal{L}$, related to the first derivative of the symmetry energy as defined in Eq. (5). Above the saturation point, the behaviors of the EOS are remarkably different, especially in the case of pure neutron matter.

2. In our calculations, all the 16 nuclei investigated are bound. This MF prediction could be in contrast with the experimental evidence. We have already mentioned the fact that, experimentally, the neutron drip line for the oxygen isotopes starts with the ^{26}O nucleus, therefore ^{28}O is an unstable system that decays by means of the strong interaction.

3. The proton s.p. energies around the Fermi surface have similar values for all the three calculations. For each isotope chain considered, the protons are more bound when the neutron number increases.

4. In each isotope chain, the energy available to arrange the proton s.p. levels decreases with increasing neutron number. As a consequence the density of states increases. We found larger density of states in non-relativistic results than in the relativistic ones.

5. The study of the density distributions indicates a good agreement at the nuclear surface for all the three types of calculations. In some isotopes, we have observed very different behaviors in the nuclear interior when the proton and neutron densities are separately considered. These differences in the nuclear center are much smaller when the total matter distribution is considered.

6. The large differences of the proton distributions in the nuclear interior are due to the s proton waves. For the calcium isotopes, we have calculated $(\mathrm{e},\mathrm{e}'\mathrm{p})$ cross sections for the knock-out of a proton from the $2s_{1/2}$ level in the kinematics of NIKHEF experiments [65]. Despite the remarkable differences in the wave functions describing the $2s_{1/2}$ levels, the three calculations produce very similar $(\mathrm{e},\mathrm{e}'\mathrm{p})$ cross sections. The comparison with the ^{40}Ca and ^{48}Ca experimental data indicates that all the results require the same quenching factor to reproduce them. Calculations of elastic electron scattering cross sections show significant differences between the various results for momentum transfer values larger than 400 MeV/c. Since the NIKHEF kinematics barely reach this value, the differences between the various s.p. wave functions used in our calculations do not produce detectable effects.

7. The values of the rms charge radii are very similar in all the three calculations and agree very well with the available experimental data and with their empirical extrapolations. Our results show a small increase of these radii with the neutron numbers.

8. We found an almost linear dependence of the neutron skins on the relative neutron excess. The relativistic calculations generated slightly larger skins than the other approaches. For comparable values of the relative neutron excess, we found larger neutron skins in lighter than in heavier nuclei. This is not a trivial geometrical effect.

Our investigation has been conducted for a specific set of nuclei where deformations are absent and pairing effects negligible. In this case, we have found a large convergence of the results of the three MF models for all the nuclei investigated, also for those nuclei not yet experimentally explored. For this reason we think that producing and investigating this type of exotic nuclei is important also from the theoretical point of view. The comparison between the observed properties and the MF predictions can confirm, or invalidate, the MF model itself, and not a specific implementation of it.

ACKNOWLEDGMENTS

This work has been partially supported by the PRIN (Italy) *Struttura e dinamica dei nuclei fuori dalla valle di stabilità*, by the Spanish Ministerio de Ciencia e Innovación under Contract Nos. FPA2009-14091-C02-02 and ACI2009-1007, and by the Junta de Andalucía (Grant No. FQM0220).

[1] http://www.rarf.riken.go.jp/eng/facilities/ribf.html.
[2] http://www-win.gsi.de/r3b/.
[3] http://www.nscl.msu.edu/features/facility-rare-isotope-beams-frib.
[4] http://www.ganil-spiral2.eu/.
[5] http://spes.lnl.infn.it/.
[6] S. C. Pieper, R. B. Wiringa, Ann. Rev. Nucl. Part. Sc. 51 (2001) 53.
[7] H. Kamada, et al., Phys. Rev. C 64 (2001) 044001.
[8] D. J. Dean, M. Hjorth-Jensen, Phys. Rev. C 69 (2004) 054320.
[9] S. Gandolfi, F. Pederiva, S. Fantoni, K. E. Schmidt, Phys. Rev. C 73 (2006) 044304.
[10] F. Arias de Saavedra, C. Bisconti, G. Co', A. Fabrocini, Phys. Rep. 450 (2007) 1.
[11] G. Hagen, T. Papenbrock, D. J. Dean, M. Hjorth-Jensen, Phys. Rev. Lett. 101 (2008) 092502.
[12] S. Quaglioni, P. Navrátil, Phys. Rev. C 79 (2009) 044606.
[13] R. Roth, T. Neff, H. Feldmeier, Prog. Part. Nucl. Phys. 65 (2010) 50.
[14] J. Speth, E. Werner, W. Wild, Phys. Rep. 33 (1977) 127.
[15] S. Kamerdzhiev, J. Speth, G. Tertychny, Phys. Rep. 393 (2004) 1.
[16] F. Grümmer, J. Speth, Jour. Phys. G 32 (2006) R193.
[17] M. Bender, P. H. Heenen, P. G. Reinhard, Rev. Mod. Phys. 75 (2003) 121.
[18] D. Vretenar, A. V. Afanasjev, G. A. Lalazissis, P. Ring, Phys. Rep. 409 (2005) 101.
[19] J. R. Stone, D. Vretenar, Prog. Part. Nucl. Phys. 58 (2007) 587.
[20] T. H. R. Skyrme, Phil. Mag. 1 (1956) 1043.
[21] T. H. R. Skyrme, Nucl. Phys. 9 (1958) 615.
[22] D. Vautherin, D. M. Brink, Phys. Rev. C 5 (1972) 626.
[23] J. Dechargè, D. Gogny, Phys. Rev. C 21 (1980) 1568.
[24] B. D. Serot, J. D. Walecka, Adv. Nucl. Phys. 16 (1986) 1.
[25] G. Co', A. M. Lallena, Phys. Rev. C 57 (1998) 145.
[26] S. Typel, H. H. Wolter, Nucl. Phys. A 656 (1999) 331.
[27] J. Meyer, Ann. Phys. Fr. 28 (2003) 1.
[28] E. Chabanat, P. Bonche, P. Haensel, J. Meyer, R. Chaeffer, Nucl. Phys. A 627 (1997) 710.
[29] E. Chabanat, P. Bonche, P. Haensel, J. Meyer, R. Chaeffer, Nucl. Phys. A 635 (1997) 231.
[30] E. Chabanat, P. Bonche, P. Haensel, J. Meyer, R. Chaeffer, Nucl. Phys. A 643 (1997) 441.
[31] J. F. Berger, M. Girod, D. Gogny, Comp. Phys. Commun. 63 (1991) 365.
[32] F. Chappert, Nouvelles paramétrisation de l'interaction nucléaire effective de Gogny, Ph.D. thesis, Université de Paris-Sud XI (France), http://tel.archives-ouvertes.fr/tel-001777379/en/ (2007).
[33] F. Chappert, M. Girod, S. Hilaire, Phys. Lett. B 668 (2008) 420.
[34] S. Goriely, S. Hilaire, M. Girod, S. Péru, Phys. Rev. Lett. 102 (2009) 242501.
[35] G. A. Lalazissis, T. Nikšić, D. Vretenar, P. Ring, Phys. Rev. C 71 (2005) 024312.
[36] S. Hilaire, M. Girod, Eur. Phys. J. A 33 (2000) 237.
[37] J. P. Delaroche, M. Girod, J. Libert, H. Goutte, S. Hilaire, S. Péru, N. Pillet, G. F. Bertsch, Phys. Rev. C 81 (2010) 014303.
[38] A. Schiller, T. Baumann, J. Dietrich, S. Kaiser, W. Peters, M. Thoennessen, Phys. Rev. C 72 (2005) 037601.
[39] B. A. Brown, Phys. Rev. Lett. 85 (2000) 5296.
[40] S. Gandolfi, A. Y. Illarionov, S. Fantoni, J. C. Miller, F. Pederiva, K. E. Schmidt, Mont. Not. R. Astron. Soc. 404 (2010) L35.
[41] A. Akmal, V. R. Pandharipande, D. G. Ravenhall, Phys. Rev. C 58 (1998) 1804.
[42] G. Audi, A. H. Wapstra, C. Thibault, Nucl. Phys. A 729 (2003) 337.
[43] P. Ring, P. Schuck, The nuclear many-body problem, Springer, Berlin, 1980.
[44] V. De Donno, G. Co', M. Anguiano, A. M. Lallena, Phys. Rev. C 83 (2011) 044324.
[45] J. Mougey, et al., Nucl. Phys. A 262 (1976) 461.
[46] M. Bernheim, et al., Nucl. Phys. A 375 (1982) 381.
[47] S. Frullani, J. Mougey, Adv. Nucl. Phys 14 (1984) 1.
[48] P. K. A. de Witt Huberts, J. Phys. G 16 (1990) 507.
[49] L. Lapikas, Nucl. Phys. A 553 (1993) 297c.
[50] S. Boffi, C. Giusti, F. D. Pacati, Phys. Rep. A 226 (1993) 1.
[51] K. I. Blomqvist, et al., Phys. Lett. B 344 (1995) 85.
[52] S. Boffi, C. Giusti, F. D. Pacati, M. Radici, Electromagnetic response of atomic nuclei, Clarendon, Oxford, 1996.
[53] C. Giusti, F. D. Pacati, Nucl. Phys. A 473 (1987) 717.
[54] C. Giusti, F. D. Pacati, Nucl. Phys. A 485 (1988) 461.
[55] A. Picklesimer, J. W. Van Orden, S. J. Wallace, Phys. Rev. C 32 (1985) 1312.
[56] J. M. Udías, P. Sarriguren, E. Moya de Guerra, E. Garrido, J. A. Caballero, Phys. Rev. C 48 (1993) 2731.
[57] J. M. Udías, P. Sarriguren, E. Moya de Guerra, J. A. Caballero, Phys. Rev. C 53 (1996) R1488.
[58] J. J. Kelly, Phys. Rev. C 56 (1997) 2672.

[59] J. M. Udías, J. A. Caballero, E. Moya de Guerra, J. E. Amaro, T. W. Donnelly, Phys. Rev. Lett. 83 (1999) 5451.
[60] A. Meucci, C. Giusti, F. D. Pacati, Phys. Rev. C 64 (2001) 014604.
[61] A. Meucci, C. Giusti, F. D. Pacati, Phys. Rev. C 64 (2001) 064615.
[62] A. Meucci, Phys. Rev. C 65 (2002) 044601.
[63] A. Meucci, C. Giusti, F. D. Pacati, Phys. Rev. C 66 (2002) 034610.
[64] M. Radici, A. Meucci, W. H. Dickhoff, Eur. Phys. Jou. A 17 (2003) 65.
[65] G. J. Kramer, The proton spectral function of ^{40}Ca and ^{48}Ca studied with the (e,e′p) reaction, Ph.D. thesis, Universiteit Amsterdam (Nederlands), unpublished (1990).
[66] C. Giusti, A. Meucci, F. D. Pacati, G. Co', V. De Donno, Phys. Rev. C 84 (2011) 024615.
[67] T. de Forest Jr., Nucl. Phys. A 392 (1983) 232.
[68] R. Anni, G. Co', P. Pellegrino, Nucl. Phys. A 584 (1995) 35.
[69] R. Anni, G. Co', Nucl. Phys. A 588 (1995) 463.
[70] B. B. P. Sinha, G. Peterson, R. R. Whitney, I. Sick, J. McCarthy, Phys. Rev. C 7 (1973) 1930.
[71] I. Sick, J. Bellicard, J. Cavedon, B. Frois, M. Huet, P. Leconte, P. Ho, S. Platchkov, Phys. Lett. B 88 (1979) 245.
[72] J. M. Cavedon, Ph.D. thesis, Université de Paris-Sud (France), unpublished (1980).
[73] I. Sick, Model-independent densities of s/d-shell nuclei, unpublished (1975).
[74] I. Sick, private communication.
[75] I. Angeli, Atomic Data and Nuclear Data Tables 87 (2004) 185.
[76] J. Piekarewicz, M. Centelles, X. Roca-Maza, X. Viñas, Eur. Phys. J. 46 (2010) 379.
[77] C. J. Pethick, D. G. Ravenhall, Nucl. Phys. A 606 (1996) 173.
[78] P. Sarriguren, M. K. Gaidarov, E. Moya de Guerra, A. N. Antonov, Phys. Rev. C 76 (2007) 044322.
[79] M. Warda, X. Viñas, X. Roca-Maza, M. Centelles, Phys. Rev. C 80 (2009) 024316.